



Heriot-Watt University
Research Gateway

Bayesian nonlinear hyperspectral unmixing with spatial residual component analysis

Citation for published version:

Altmann, Y, Pereyra, M & McLaughlin, S 2015, 'Bayesian nonlinear hyperspectral unmixing with spatial residual component analysis', *IEEE Transactions on Computational Imaging*, vol. 1, no. 3, pp. 174 - 185. <https://doi.org/10.1109/TCI.2015.2481603>

Digital Object Identifier (DOI):

[10.1109/TCI.2015.2481603](https://doi.org/10.1109/TCI.2015.2481603)

Link:

[Link to publication record in Heriot-Watt Research Portal](#)

Document Version:

Early version, also known as pre-print

Published In:

IEEE Transactions on Computational Imaging

General rights

Copyright for the publications made accessible via Heriot-Watt Research Portal is retained by the author(s) and / or other copyright owners and it is a condition of accessing these publications that users recognise and abide by the legal requirements associated with these rights.

Take down policy

Heriot-Watt University has made every reasonable effort to ensure that the content in Heriot-Watt Research Portal complies with UK legislation. If you believe that the public display of this file breaches copyright please contact open.access@hw.ac.uk providing details, and we will remove access to the work immediately and investigate your claim.

Bayesian nonlinear hyperspectral unmixing with spatial residual component analysis

Yoann Altmann, Marcelo Pereyra and Stephen McLaughlin

Abstract

This paper presents a new Bayesian model and algorithm for nonlinear unmixing of hyperspectral images. The model proposed represents the pixel reflectances as linear combinations of the endmembers, corrupted by nonlinear (with respect to the endmembers) terms and additive Gaussian noise. Prior knowledge about the problem is embedded in a hierarchical model that describes the dependence structure between the model parameters and their constraints. In particular, a gamma Markov random field is used to model the joint distribution of the nonlinear terms, which are expected to exhibit significant spatial correlations. An adaptive Markov chain Monte Carlo algorithm is then proposed to compute the Bayesian estimates of interest and perform Bayesian inference. This algorithm is equipped with a stochastic optimisation adaptation mechanism that automatically adjusts the parameters of the gamma Markov random field by maximum marginal likelihood estimation. Finally, the proposed methodology is demonstrated through a series of experiments with comparisons using synthetic and real data and with competing state-of-the-art approaches.

Keywords

Hyperspectral imagery, nonlinear spectral unmixing, residual component analysis, Gamma Markov random field, Bayesian estimation.

I. INTRODUCTION

Spectral unmixing (SU) is a key problem in the analysis of hyperspectral images. This is a source separation problem consisting of recovering the spectral signatures (endmembers) of

This study was supported by the Direction Générale de l'armement, French Ministry of Defence, by the SuSTaIN program - EPSRC grant EP/D063485/1 - at the Department of Mathematics, University of Bristol, and the EPSRC via grant EP/J015180/1.

Y. Altmann and S. McLaughlin are with the School of Engineering and Physical Sciences, Heriot-Watt University, Edinburgh U.K. (email: {Y.Altmann,S.McLaughlin}@hw.ac.uk).

M. Pereyra is with the School of Mathematics of the University of Bristol, Bristol U.K. (email: marcelo.pereyra@bristol.ac.uk).

the materials present in the scene, and quantifying their proportions within each hyperspectral image pixel. The SU problem has been widely studied for images where pixel reflectances are linear combinations of pure component spectra [1], [2]. However, it is now widely accepted that the linear mixing model (LMM) can be inappropriate for some hyperspectral images, particularly those containing sand-like materials or relief. Several nonlinear mixing models (NLMM) have been recently proposed to address the limitations of the LMM. There are two main approaches to dealing with NLMM. The first seeks to model the physics of the image formation model (e.g., *intimate mixtures* [3] for short-range multiple light scattering, and polynomial models for long-range multiple light scattering [4]–[6]). The second seeks to construct flexible models that can represent a wide range of nonlinearities. This can be achieved using neural networks, kernel functions [7], or post-nonlinear transformations [8], [9] for instance.

While the consideration of nonlinear effects can be very relevant in some specific regions of the scene, most hyperspectral image pixels are well described by the LMM. Therefore, models for nonlinear unmixing should include the LMM as a special case. Here we use a variation of the Bayesian NLMM proposed recently in Altmann et al. [10], which is inspired by residual component analysis (RCA) [11]. In that model the nonlinear effects in hyperspectral images are represented as additive perturbations (of the LMM) that are modelled as a collection of Gaussian processes (GPs) equipped with a hidden Potts-Markov random field (MRF) partitioning the image into regions sharing the same GP. The model of [10] has two drawbacks that we address in this paper. First, the Potts model constrains nonlinearities to take a finite number of possible energy states (the so-called *nonlinearity levels*); this number is difficult to specify a priori unless there is very accurate knowledge about the nonlinearities present in the scene. Second, in [10] nonlinearities are allowed to take negative values, as this allows marginalising them analytically (i.e., integrating them out of the model) and thus simplifies the statistical inference procedure; however, our experiments suggest that taking into account the positivity of the nonlinearities significantly improves the estimation results. Here we address these drawbacks by replacing the Potts MRF by a gamma MRF model [12] that encodes the positivity of the nonlinearities and also allows an infinite number of levels of nonlinearity.

The remainder of the paper is organised as follows. Section II recalls the RCA model for hyperspectral image unmixing. The Bayesian NLMM proposed in this paper is presented in Section III. In Section IV we propose a Markov chain Monte Carlo Bayesian algorithm

to perform statistical inference in this model and we define Bayesian estimators for non-linear unmixing and nonlinearity detection. Sections V and VI demonstrate the proposed methodology through a series of experiments with synthetic and real hyperspectral images and comparisons with methods from the state of the art. Conclusions and perspectives for future work are finally reported in Section VII.

II. PROBLEM FORMULATION

Let $\mathbf{y}_{i,j} \in \mathbb{R}^L$ be the pixel at location (i, j) of an hyperspectral image \mathbf{Y} of size $N_{\text{row}} \times N_{\text{col}}$ and observed at L spectral bands. We model each image pixel as a linear combination of R known spectra or endmembers \mathbf{m}_r , plus an additive perturbation $\phi_{i,j}$ embedding nonlinearities and additive noise

$$\begin{aligned} \mathbf{y}_{i,j} &= \sum_{r=1}^R a_{r,i,j} \mathbf{m}_r + \phi_{i,j} + \mathbf{e}_{i,j} \\ &= \mathbf{M} \mathbf{a}_{i,j} + \phi_{i,j} + \mathbf{e}_{i,j}, \quad \forall (i, j) \end{aligned} \quad (1)$$

where $\mathbf{m}_r = [m_{r,1}, \dots, m_{r,L}]^T$ is the spectral response of the r th material present in the scene, $a_{r,i,j}$ is its abundance within pixel (i, j) and $\mathbf{e}_n \sim \mathcal{N}(\mathbf{0}_L, \Sigma_0)$ is Gaussian noise with diagonal covariance matrix $\Sigma_0 = \text{diag}(\boldsymbol{\sigma}^2)$ with elements $\boldsymbol{\sigma}^2 = [\sigma_1^2, \dots, \sigma_L^2]^T$ (note that matrix and vector notations $\mathbf{M} = [\mathbf{m}_1, \dots, \mathbf{m}_R]$ and $\mathbf{a}_{i,j} = [a_{1,i,j}, \dots, a_{R,i,j}]^T$ have been used in the second row of (1)). Due to physical considerations we model the abundances as non-negative quantities and set $a_{r,i,j} \in \mathbb{R}^+$ (notice that because we consider non-linear mixing we do not use the sum-to-one constraint that is commonly enforced in linear mixing models). Moreover, for the nonlinear effects we use the deterministic model

$$\phi_{i,j} = \phi(\boldsymbol{\gamma}_{i,j}) = \sum_{k=1}^{R-1} \sum_{k'=k+1}^R \gamma_{i,j}^{(k,k')} \sqrt{2} \mathbf{m}_k \odot \mathbf{m}_{k'} + \sum_{k=1}^R \gamma_{i,j}^{(k)} \mathbf{m}_k \odot \mathbf{m}_k. \quad (2)$$

that is parametrised by a vector $\boldsymbol{\gamma}_{i,j} = [\gamma_{i,j}^{(1,2)}, \dots, \gamma_{i,j}^{(R-1,R)}, \gamma_{i,j}^{(1)}, \dots, \gamma_{i,j}^{(R)}]^T$ of nonlinearity coefficients of length $K = R(R+1)/2$. Again, we assume that $\gamma_{i,j} \in \mathbb{R}^+$. This model is motivated by the fact that nonlinearities in hyperspectral images are well represented as polynomial interactions between endmembers (see [5], [6], [8], [13] for more details).

This paper considers the inverse problems of estimating the abundances $\mathbf{a}_{i,j}$ and of detecting the presence of nonlinearities at each image pixel $\mathbf{y}_{i,j}$ (whose intensity can then be measured by estimating $\|\boldsymbol{\gamma}_{i,j}\|_2^2$). We formulate this problem as a statistical inference task that we address in a Bayesian framework by defining an appropriate Bayesian model and inference algorithm.

III. BAYESIAN MODEL

This section presents an original Bayesian model for inferring the unknown quantities of interest \mathbf{A} and $\mathbf{\Gamma}$ from the observed hyper-spectral image \mathbf{Y} , where \mathbf{A} is an $R \times N_{\text{row}} \times N_{\text{col}}$ array gathering the abundance vectors $\mathbf{a}_{i,j}$ and $\mathbf{\Gamma}$ an $K \times N_{\text{row}} \times N_{\text{col}}$ array gathering the nonlinearity coefficient vectors $\gamma_{i,j}$. Following a hierarchical Bayesian approach, we also include in the model all the parameters of the model whose values are not easily known a priori and need to be inferred from data jointly with \mathbf{A} and $\mathbf{\Gamma}$ (e.g., the noise covariance σ^2). Unlike \mathbf{A} and $\mathbf{\Gamma}$, the other unknown quantities are of no interest for decision making and are therefore removed from the model by marginalisation during the inference procedure.

A. Likelihood

From the non-linear mixing model (1), and by assuming that observations $\mathbf{Y} = [\mathbf{y}_1, \dots, \mathbf{y}_N]$ are conditionally independent given $\mathbf{A}, \mathbf{\Gamma}$ and σ^2 , we obtain

$$f(\mathbf{Y}|\mathbf{A}, \mathbf{\Gamma}, \sigma^2) \propto \prod_{i,j} |\Sigma_0|^{-1/2} \exp \left[-\frac{(\mathbf{y}_{i,j} - \mathbf{x}_{i,j})^T \Sigma_0^{-1} (\mathbf{y}_{i,j} - \mathbf{x}_{i,j})}{2} \right] \quad (3)$$

with $\mathbf{x}_{i,j} = \mathbf{M}\mathbf{a}_{i,j} + \phi(\gamma_{i,j})$, $\Sigma_0 = \text{diag}(\sigma^2)$, and where \propto denotes proportionality. Note that to lighten notation the dependence on \mathbf{M} is not denoted explicitly (\mathbf{M} is assumed to be perfectly known).

B. Prior for the abundance matrix \mathbf{A}

We assign the abundance coefficients the following hierarchical prior distribution

$$a_{r,i,j} | \beta_r \sim \mathcal{N}_{\mathbb{R}^+}(0, \beta_r) \quad (4)$$

$$\beta_r \sim \mathcal{IG}(\alpha_1, \alpha_2) \quad (5)$$

parametrised by some fixed hyper-parameters α_1 and α_2 , and where we note that the prior on $a_{r,i,j} | \beta_r$ is truncated to \mathbb{R}^+ to reflect the positivity of $a_{r,i,j}$. This prior is very flexible and can be adjusted to represent a wide variety of prior beliefs. Here we set $\alpha_1 = 1$ leading to a (marginal) exponential prior for $a_{r,i,j}$. This represents the fact that we expect abundances to be sparse (at least approximately), given that most materials are not present on all image pixels. The value of α_2 has little impact on the inferences given the high-dimensionality of \mathbf{A} . Here we set $\alpha_2 = 2$ to model the fact that abundances often take values in $[0, 1]$.

Notice that a strength of a hierarchical prior such as (4) is their natural capacity to encode prior dependences between unknown variables. For example, we expect the abundance

coefficients associated with the same material to exhibit correlations, in particular in terms of their scale. This belief is encoded in (4) by defining one hidden variable β_r for each material or endmember \mathbf{m}_r , which is shared by all the abundances related to that material. This hierarchical structure operates as a global pooling mechanism that shares information across the rows of \mathbf{A} (i.e, the abundance coefficients associated to the r th material).

Finally, assuming that abundances are prior independent given the hidden variables $\boldsymbol{\beta} = [\beta_1, \dots, \beta_R]^T$, we obtain the following following joint prior for $\mathbf{A}, \boldsymbol{\beta}$

$$f(\mathbf{A}, \boldsymbol{\beta}) = f(\mathbf{A}|\boldsymbol{\beta})f(\boldsymbol{\beta}) \quad (6)$$

with $f(\mathbf{A}|\boldsymbol{\beta}) = \prod_{r,i,j} f(a_{r,i,j}|\beta_r)$ and $f(\boldsymbol{\beta}) = \prod_r f(\beta_r|\alpha_1, \alpha_2)$. Also notice that by using the hierarchical structure (4) we obtain conjugate priors and hyper-priors for $a_{r,i,j}$ and β_r . Conjugacy generally leads to inference algorithms with significantly better tractability and computational efficiency, which is crucial given the high dimensionality of \mathbf{A} .

C. Priors for the nonlinearity coefficients $\boldsymbol{\Gamma}$

One of the contributions of this paper is to propose the following hierarchical prior for the nonlinearity coefficients

$$\begin{cases} \gamma_{i,j}|s_{i,j} \sim \mathcal{N}_{(\mathbb{R}^+)^K}(\mathbf{0}, s_{i,j}\mathbf{I}_K) \\ s_{i,j} \sim \mathcal{IG}(\alpha_3, \alpha_3\alpha_{4,i,j}). \end{cases} \quad (7)$$

Notice that this prior is parametrized by a local hyper-parameter $\alpha_{4,i,j}$ that is related to the prior mean and mode of $s_{i,j}$ and therefore to the strength of the nonlinearities at the pixel (i, j) (via the norm $\|\boldsymbol{\gamma}_{i,j}\|_2^2$). The prior also depends on a global hyper-parameter α_3 that controls the shape of the tails and in particular the deviation of $s_{i,j}$ from $\alpha_{4,i,j}$.

As explained previously, a key feature of hierarchical models is their capacity to encode dependence and act as pooling mechanisms that share information across covariates to improve the inference. We wish to specify (7) to reflect the prior belief that nonlinearities exhibit spatial correlations. In particular, due to the spatial organisation of images, we expect the values of $\gamma_{i,j}$ to vary smoothly from one pixel to another. In order to model this behaviour we specify $\alpha_{4,i,j}$ such that the resulting prior for $\boldsymbol{\Gamma}$ is a hidden gamma-Markov random field (GMRF) [12].

More precisely, we denote by \mathbf{S} the $N_{\text{row}} \times N_{\text{col}}$ matrix with elements $s_{i,j}$, introduce a $(N_{\text{row}} + 1) \times (N_{\text{col}} + 1)$ auxiliary matrix \mathbf{W} with elements $w_{i,j} \in \mathbb{R}^+$ and define a bipartite conditional independence graph between \mathbf{S} and \mathbf{W} such that each $s_{i,j}$ is connected to four

neighbour elements of \mathbf{W} and vice-versa. This 1st order neighbourhood structure is depicted in Fig.1, where we notice that any given $s_{i,j}$ and $s_{i+1,j}$ are 2nd order neighbours via $w_{i,j+1}$ and $w_{i+1,j+1}$. We specify a GMRF prior for \mathbf{S}, \mathbf{W} [12], and obtain the following hierarchical prior for $\Gamma, \mathbf{S}, \mathbf{W}$

$$\gamma_{i,j}|s_{i,j} \sim f(\gamma_{i,j}|s_{i,j}) \quad (8a)$$

$$s_{i,j}|\mathbf{W}, \alpha_3 \sim \mathcal{IG}(\alpha_3, \alpha_3 \alpha_{4,i,j}(\mathbf{W})) \quad (8b)$$

$$w_{i,j}|\mathbf{S}, \alpha_3 \sim \mathcal{G}(\alpha_3, 1/(\alpha_3 \alpha_{5,i,j}(\mathbf{S}))) \quad (8c)$$

where

$$\alpha_{4,i,j}(\mathbf{W}) = w_{i,j} + w_{i+1,j} + w_{i,j+1} + w_{i+1,j+1}/4$$

$$\alpha_{5,i,j}(\mathbf{W}) = (s_{i,j}^{-1} + s_{i-1,j}^{-1} + s_{i,j-1}^{-1} + s_{i-1,j-1}^{-1})/4.$$

The density for this joint prior for Γ, \mathbf{S} and \mathbf{W} is given by

$$f(\Gamma, \mathbf{S}, \mathbf{W}|\alpha_3) = f(\Gamma|\mathbf{S})f(\mathbf{S}, \mathbf{W}|\alpha_3)$$

where $f(\Gamma|\mathbf{S}) = \prod_{i,j} f(\gamma_{i,j}|s_{i,j})$ and

$$\begin{aligned} f(\mathbf{S}, \mathbf{W}|\alpha_3) &= \frac{1}{Z(\alpha_3)} \prod_{(i,j) \in \mathcal{V}_{\mathbf{S}}} (s_{i,j})^{-(\alpha_3+1)} \\ &\times \prod_{(i',j') \in \mathcal{V}_{\mathbf{W}}} w_{i',j'}^{(\alpha_3-1)} \\ &\times \prod_{((i,j),(i',j')) \in \mathcal{E}} \exp\left(\frac{-\alpha_3 w_{i',j'}}{4s_{i,j}}\right). \end{aligned} \quad (9)$$

Notice that we denote explicitly the dependence on the value of α_3 , which here acts a regularisation parameter that controls the amount of spatial smoothness enforced by the GMRF. Following an empirical Bayesian approach, the value of α_3 remains unspecified and will be adjusted automatically during the inference procedure by maximum marginal likelihood estimation.

Finally, it is worth mentioning that this model for the nonlinearity coefficients has similarities with the model proposed in [10] that also considers the spatial regularity of nonlinearities. However, the model described [10] follows a segmentation approach in which the non-linearity coefficients are assumed (and constrained) to take values in a finite set. This leads to a piece-wise constant representation and requires specification of the number of nonlinearity levels present in the image, a value that is often difficult to determine a

priori. The model proposed in this paper provides a spatially smooth representation of the nonlinearities that is possibly more realistic than the piece-wise constant representation of [10], and also has the practical advantage of not requiring practitioners to specify the finite number of admissible nonlinearity levels. Another important distinction is that the model described in [10] does not take into account the positivity of $\gamma_{i,j}$, which we have found to greatly improve the estimation of the nonlinearities.

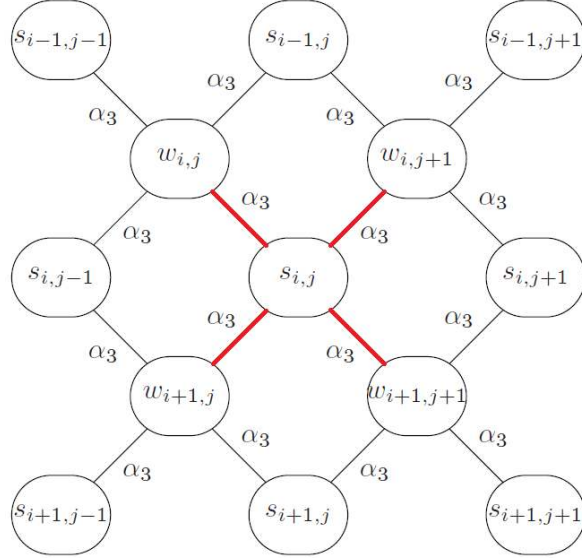


Fig. 1. Proposed 1st order neighbourhood structure ($\forall(i, j) \in \Omega$).

D. Prior for the noise covariance σ^2

We assume that there is no prior knowledge available about the values of noise covariance (other than the fact that it is diagonal) and assign each diagonal element σ_ℓ^2 a Jeffreys' prior, leading to the joint prior

$$f(\boldsymbol{\sigma}^2) = \prod_{\ell=1}^L f(\sigma_\ell^2), \quad \text{with} \quad f(\sigma_\ell^2) \propto \sigma_\ell^{-2} \mathbf{1}_{\mathbb{R}^+}(\sigma_\ell^2). \quad (10)$$

In scenarios where prior knowledge is available, practitioners can incorporate this information into the model by replacing the Jeffreys' prior by a more informative model (e.g. a conjugate inverse-Gamma distribution).

E. Posterior distribution

We are now ready to specify the posterior distribution for \mathbf{A} , $\boldsymbol{\Gamma}$, $\boldsymbol{\sigma}^2$, \mathbf{S} , \mathbf{W} and $\boldsymbol{\beta}$ given the observed hyper-spectral image \mathbf{Y} and the value of the spatial regularisation hyper-parameter

α_3 (recall that this value will be determined by maximum marginal likelihood estimation during the inference procedure). Using Bayes' theorem, and assuming prior independence between $(\mathbf{A}, \boldsymbol{\beta})$, $(\boldsymbol{\Gamma}, \mathbf{S}, \mathbf{W})$ and σ^2 , the joint posterior distribution associated with the proposed Bayesian model is given by

$$f(\mathbf{A}, \boldsymbol{\Gamma}, \sigma^2, \mathbf{S}, \mathbf{W}, \boldsymbol{\beta} | \mathbf{Y}, \alpha_3) \propto f(\mathbf{Y} | \mathbf{A}, \boldsymbol{\Gamma}, \sigma^2) f(\mathbf{A} | \boldsymbol{\beta}) f(\boldsymbol{\beta}) f(\boldsymbol{\Gamma} | \mathbf{S}) f(\mathbf{S}, \mathbf{W} | \alpha_3). \quad (11)$$

For illustration, Fig. 2 depicts the directed acyclic graph (DAG) summarising the structure proposed Bayesian model (recall that \mathbf{S}, \mathbf{W} have a bi-partite neighbourhood structure, which is illustrated in the graphical model of Fig. 1).

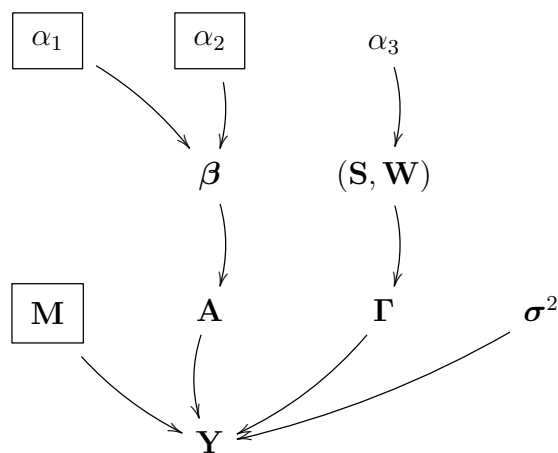


Fig. 2. Graphical model for the proposed hierarchical Bayesian model (fixed quantities appear in boxes).

IV. BAYESIAN INFERENCE

A. Bayesian estimators

The Bayesian model defined in Section III specifies the joint posterior density for the unknown parameters $\mathbf{A}, \boldsymbol{\Gamma}, \sigma^2, \mathbf{S}, \mathbf{W}$ and $\boldsymbol{\beta}$ given the observed quantities \mathbf{Y}, \mathbf{M} and the hyperparameter α_3 . This posterior distribution models our complete knowledge about the unknowns given the observed data and the prior information available. In this section we define suitable Bayesian estimators to summarise this knowledge and perform hyperspectral unmixing. More precisely, we propose the following two Bayesian estimators for hyperspectral non-linear unmixing and nonlinearity estimation and detection: The marginal posterior mean or minimum mean square error estimator of the abundance matrix

$$\hat{\mathbf{A}}_{\text{MMSE}} = \mathbb{E}[\mathbf{A} | \mathbf{Y}, \hat{\alpha}_3], \quad (12)$$

where the expectation is taken with respect to the marginal posterior density $f(\mathbf{A}|\mathbf{Y}, \alpha_3)$ (by marginalising $\Gamma, \sigma^2, \mathbf{S}, \mathbf{W}$ and β this density takes into account their uncertainty). The minimum mean square error estimator of the pixel-wise nonlinearity energy

$$\left(\widehat{\|\phi_{i,j}\|_2^2} \right)_{\text{MMSE}} = \mathbb{E} \left[\|\phi_{i,j}\|_2^2 | \mathbf{Y}, \hat{\alpha}_3 \right], \quad (13)$$

where the expectation is now taken with respect to $f(\|\phi_{i,j}\|_2^2 | \mathbf{Y}, \alpha_3)$. And the Bayesian hypothesis test for nonlinearity detection

$$P_{i,j} > a_1 / (a_0 + a_1),$$

where

$$P_{i,j} = \mathbb{E} [T_{i,j}(\phi_{i,j}, \mathbf{a}_{i,j}) > \eta | \mathbf{Y}, \hat{\alpha}_3], \quad (14)$$

with

$$T_{i,j}(\phi_{i,j}, \mathbf{a}_{i,j}) = \frac{\|\phi_{i,j}\|_2^2}{\|\mathbf{y}_{i,j} - \mathbf{M}\mathbf{a}_{i,j} - \phi_{i,j}^{(t)}\|_2^2},$$

is the posterior probability that the power of the nonlinear effects in pixel (i, j) is η times larger than the power of the noise at that pixel, and where a_0 and a_1 are application-specific weights associated with incorrectly rejecting or accepting this hypothesis (in our experiments we have used $a_0 = a_1, \eta = 2$).

Notice that in (12), (13) and (14) we have set $\alpha_3 = \hat{\alpha}_3$, which denotes the maximum marginal likelihood estimator of the MRF regularisation hyper-parameter α_3 given the observed data \mathbf{Y} , i.e.,

$$\hat{\alpha}_3 = \underset{\alpha_3 \in \mathbb{R}^+}{\operatorname{argmax}} f(\mathbf{Y} | \alpha_3), \quad (15)$$

This approach for specifying α_3 is taken from the empirical Bayes framework in which hyper-parameters with unknown values are replaced by point estimates computed from observed data (as opposed to being fixed a priori or integrated out of the model by marginalisation). As explained in [14], this strategy has several important advantages for MRF hyper-parameters with doubly intractable conditional distributions such as α_3 . In particular, it allows for the automatic adjustment of the value of α_3 for each image (thus producing significantly better estimation results than using a single fixed value of α_3 for all images), and has a computational cost that is several times lower than that of competing approaches, such as including α_3 in the model and subsequently marginalising it during the inference procedure [15].

B. Bayesian algorithm

Computing the estimators (12), (13) and (14) is very challenging because it involves calculating expectations with respect to posterior marginal densities, which in turn require evaluating the full posterior (11) and integrating it over a very high-dimensional space. Computing $\hat{\alpha}_3$ is also difficult because it involves solving an intractable optimisation problem, (because it is not possible to evaluate the marginal likelihood $f(\mathbf{Y}|\alpha_3)$ or its gradient $\nabla f(\mathbf{Y}|\alpha_3)$). Here we adopt the approach proposed in [14] and design a stochastic optimisation and simulation algorithm to compute (12), (13), (14) and (11) simultaneously. That is, we construct a stochastic gradient Markov chain Monte Carlo (SGMCMC) algorithm that simultaneously estimates $\hat{\alpha}_3$ and generates a chain of N_{MC} samples $\{\mathbf{A}^{(t)}, \mathbf{\Gamma}^{(t)}, \mathbf{S}^{(t)}\}_{t=1}^{N_{\text{MC}}}$ asymptotically distributed according to the marginal density $f(\mathbf{A}, \mathbf{\Gamma}, \mathbf{S}|\mathbf{Y}, \hat{\alpha}_3)$ (this algorithm is summarised in Algo. 1 below). Once the samples have been generated, the estimators (12), (13) and (14) are approximated by Monte Carlo integration [16, Chap. 10], i.e.,

$$\hat{\mathbf{A}}_{MMSEj} = \frac{1}{N_{\text{MC}} - N_{\text{bi}}} \sum_{t=N_{\text{bi}}+1}^{N_{\text{MC}}} \mathbf{A}^{(t)}, \quad (16)$$

$$\left(\widehat{\|\phi_{i,j}\|_2^2} \right)_{MMSEj} = \frac{1}{N_{\text{MC}} - N_{\text{bi}}} \sum_{t=N_{\text{bi}}+1}^{N_{\text{MC}}} \|\phi(\gamma_{i,j}^{(t)})\|_2^2, \quad (17)$$

and

$$\hat{P}_{i,j} = \frac{1}{N_{\text{MC}} - N_{\text{bi}}} \sum_{t=N_{\text{bi}}+1}^{N_{\text{MC}}} \left[\mathbf{1}_{(\eta, \infty)}(T_{i,j}^{(t)}) \right], \quad (18)$$

with $T_{i,j}^{(t)} = \|\phi(\gamma_{i,j}^{(t)})\|_2^2 / \|\mathbf{y}_{i,j} - \mathbf{M}\mathbf{a}_{i,j} - \phi(\gamma_{i,j}^{(t)})\|_2^2$, and where the samples from the first N_{bi} iterations (corresponding to the transient regime or burn-in period) are discarded. The main steps of this algorithm are detailed in below.

1) *Sampling the mixing parameters:* The conditional distribution of $\mathbf{A}, \mathbf{\Gamma}$ given the other variables of the model is given by

$$f(\mathbf{A}, \mathbf{\Gamma}|\mathbf{Y}, \mathbf{\Psi}, \sigma^2, \alpha_3) = \prod_{i,j} f(\mathbf{a}_{i,j}, \gamma_{i,j}|\mathbf{y}_n, \mathbf{\Psi}, \sigma^2) \quad (19)$$

where

$$\mathbf{a}_{i,j}, \gamma_{i,j}|\mathbf{y}_n, \mathbf{\Psi}, \sigma^2 \sim \mathcal{N}_{(\mathbb{R}^+)^{R+K}}(\boldsymbol{\mu}_{i,j}, \boldsymbol{\Sigma}_{i,j}), \quad (20)$$

with

$$\begin{cases} \Sigma_{i,j} &= (\mathbf{R}_{i,j} + \mathbf{G}^T \Sigma_0^{-1} \mathbf{G})^{-1}, \\ \boldsymbol{\mu}_{i,j} &= \Sigma_{i,j} \mathbf{G}^T \Sigma_0^{-1} \mathbf{y}_{i,j}, \end{cases} \quad (21)$$

and where \mathbf{G} is an $L \times (R+D)$ matrix with the endmembers and the D nonlinear interaction spectra, i.e., $\mathbf{G} = [\mathbf{M}, \mathbf{m}_1 \odot \mathbf{m}_2, \dots, \mathbf{m}_{R-1} \odot \mathbf{m}_R, \mathbf{m}_1 \odot \mathbf{m}_1, \dots, \mathbf{m}_R \odot \mathbf{m}_R]$ and

$$\mathbf{R}_{i,j} = \left(\begin{bmatrix} \text{diag}(\boldsymbol{\beta}) & \mathbf{0}_{R,D} \\ \mathbf{0}_{D,R} & s_{i,j} \mathbf{I}_D \end{bmatrix} \right)^{-1}.$$

We simulate samples from (20) with the algorithm recently proposed in [17].

2) *Sampling the noise variances:* The conditional distribution of σ^2 given the other variables of the model is given by

$$f(\sigma^2 | \mathbf{Y}, \mathbf{A}, \boldsymbol{\Gamma}, \boldsymbol{\Psi}, \alpha_3) = \prod_{\ell=1}^L f(\sigma_\ell^2 | \mathbf{Y}, \mathbf{A}, \boldsymbol{\Psi}, \boldsymbol{\beta}, \alpha_3), \quad (22)$$

with

$$f(\sigma_\ell^2 | \mathbf{Y}, \mathbf{A}, \boldsymbol{\Gamma}, \mathbf{S}, \mathbf{W}, \boldsymbol{\beta}, \alpha_3) = p_{\mathcal{IG}} \left(\sigma_\ell^2; N/2, \sum_{i,j} \frac{(\mathbf{y}_{i,j} - \mathbf{x}_{i,j})^T \Sigma_0^{-1} (\mathbf{y}_{i,j} - \mathbf{x}_{i,j})}{2} \right). \quad (23)$$

Sampling from the conditional (22) is achieved by simulating L independent inverse gamma random variables.

3) *Sampling the abundance hyper-parameters:* Similarly, the elements of $\boldsymbol{\beta}$ are also conditionally independent (given the other variables of the model) and can be simulated in parallel by generating inverse gamma random variables with distribution

$$\beta_r | \mathbf{Y}, \boldsymbol{\theta}, \mathbf{S}, \mathbf{W}, a \sim \mathcal{IG} \left(\frac{N}{2} + \alpha_1, \sum_{i,j} \frac{\mathbf{a}_{i,j}^2}{2} + \alpha_2 \right). \quad (24)$$

4) *Sampling the nonlinearity levels \mathbf{S} :* Again, the elements of \mathbf{S} are conditionally independent given the other model parameters

$$f(\mathbf{S} | \mathbf{Y}, \boldsymbol{\theta}, \mathbf{W}, \alpha_3) = \prod_{(i,j) \in \mathcal{V}_\mathbf{S}} f(s_{i,j} | \mathbf{Y}, \boldsymbol{\theta}, \mathbf{W}, \alpha_3), \quad (25)$$

and can be simulated in parallel by generating inverse gamma random variables with distribution

$$s_{i,j} | \mathbf{Y}, \boldsymbol{\theta}, \mathbf{W}, \alpha_3 \sim \mathcal{IG} \left(\alpha_3 + \frac{K}{2}, \nu_{i,j} + \frac{\|\boldsymbol{\gamma}_{i,j}\|_2^2}{2} \right). \quad (26)$$

5) *Updating the MRF regularisation parameter α_3* : If marginal likelihood $f(\mathbf{Y}|\alpha_3)$ was tractable we could update α_3 from one MCMC iteration to the next by using a classic gradient descent step

$$\alpha_3^{(t+1)} = \alpha_3^{(t)} + \delta_t \nabla \log f(\mathbf{Y}|\alpha_3^{(t)}),$$

with $\delta_t = t^{-3/4}$, such that $\alpha_3^{(t)}$ converges to $\hat{\alpha}_3$ as $t \rightarrow \infty$. However, this gradient has two levels of intractability, one due to the marginalisation of $(\mathbf{A}, \mathbf{\Gamma}, \sigma^2, \mathbf{S}, \mathbf{W}, \beta)$ and another one due to the intractable normalising constant of the gamma MRF. We address this difficulty by following the approach proposed in [14]; that is, by replacing $\nabla \log f(\mathbf{Y}|\alpha_3^{(t)})$ with an estimator computed with the samples generated by the MCMC algorithm at iteration t , and a set of two auxiliary variables $(\mathbf{S}', \mathbf{W}') \sim \mathcal{K}(\mathbf{S}, \mathbf{W}|\mathbf{S}^{(t)}, \mathbf{W}^{(t)}, \alpha_3^{(t-1)})$ generated with an MCMC kernel \mathcal{K} with target density (9) (in our experiments we used a Gibbs sampler implemented using a colouring scheme such that all the elements of \mathbf{S}' and \mathbf{W}' are generated in parallel). The updated value $\alpha_3^{(t+1)}$ is then projected onto an interval $[0, A_t]$ to guarantee the positivity constraint $\alpha_3 \in \mathbb{R}^+$ and the stability of the stochastic optimisation algorithm (we have used $A_t = 20$).

It is worth mentioning that if it was possible to simulate the auxiliary variables $(\mathbf{S}', \mathbf{W}')$ exactly from (9) then the estimator of $\nabla \log f(\mathbf{Y}|\alpha_3^{(t)})$ used in Algo. 1 would be unbiased and as a result $\alpha_3^{(t)}$ would converge exactly to $\hat{\alpha}_3$. However, exact simulation from (9) is not computationally feasible and therefore we resort to the MCMC kernel \mathcal{K} and obtain a biased estimator of $\nabla \log f(\mathbf{Y}|\alpha_3^{(t)})$ that drives $\alpha_3^{(t)}$ to a neighbourhood of $\hat{\alpha}_3$ [14]. We have found that computing this biased estimator is significantly less expensive than alternative approaches, (e.g., using an approximate Bayesian computation algorithm as in [15]), and that it leads to very accurate nonlinear unmixing results.

ALGORITHM 1

Proposed MCMC algorithm

- 1: Fixed input parameters: Endmember matrix \mathbf{M} , number of burn-in iterations N_{bi} , total number of iterations N_{MC}
- 2: Initialization ($t = 0$)
 - Set $\mathbf{A}^{(0)}, \sigma^{2(0)}, \mathbf{\Gamma}^{(0)}, \mathbf{S}^{(0)}, \mathbf{W}^{(0)}, \beta^{(0)}, \alpha_3^{(0)}$
- 3: Iterations ($1 \leq t \leq N_{\text{MC}}$)
- 4: Sample $(\mathbf{A}^{(t)}, \mathbf{\Gamma}^{(t)})$ from (20)
- 5: Sample $\sigma^{2(t)}$ from (22)

```

6: Sample  $\beta^{(t)}$  from (24)
7: Sample  $\mathbf{S}^{(t)}$  from (25)
8: Sample  $\mathbf{W}^{(t)}$  from (8c)
9: if  $t < N_{\text{bi}}$  then
10:   Sample  $(\mathbf{S}', \mathbf{W}') \sim \mathcal{K}(\mathbf{S}, \mathbf{W} | \mathbf{S}^{(t)}, \mathbf{W}^{(t)}, \alpha_3^{(t-1)})$ 
11:   Set  $\alpha_3^{(t)} = \mathcal{P}_{[0, A_t]}(\alpha_3^{(t-1)} + \delta_t [\Lambda_1(\mathbf{S}, \mathbf{W}) - \Lambda_1(\mathbf{S}', \mathbf{W}')]])$ 
12: else
13:   Set  $\alpha_3^{(t)} = \alpha_3^{(t-1)}$ 
14: end if
15: Set  $t = t + 1$ .
16: Output  $\{\mathbf{A}^{(t)}, \mathbf{\Gamma}^{(t)}, \mathbf{S}^{(t)}\}_{t=1}^{N_{\text{MC}}}$ .

```

V. SIMULATIONS: SYNTHETIC DATA

In this section we study the performance of the proposed algorithm on a series of synthetic hyperspectral images firstly with linear mixing and secondly with nonlinear mixing.

A. First scenario: Linearly mixed image

The objective here is to assess whether using the nonlinear unmixing model proposed in this paper leads to good unmixing results when analysing linearly mixed images, or if the additional degrees of freedom in the model degrade the estimation performance. This is crucial because in real hyperspectral images most pixels exhibit predominantly linear mixing. We evaluate the performance of the proposed *Generalized-RCA* (G-RCA) algorithm (and its version incorporating the nonlinearity positivity constraints, referred to as G-RCA+) by unmixing a synthetic image of 100×100 pixels generated with the classical linear mixing model (i.e., (1) with $\gamma_{i,j} = 0$) and using $R = 3$ endmembers (i.e., green grass, olive green paint and galvanised steel metal)¹. This image is generated at $L = 207$ spectral bands and with an average signal to noise ratio of 30dB ($\sigma_\ell^2 = 3 \cdot 10^{-4}, \forall \ell$). The abundance vectors $\mathbf{a}_{i,j}$ used to produce this image have been generated using the model (4) (we later present another experiment where the abundances satisfy the sum-to-one constraint). The G-RCA and G-RCA+ algorithms for this experiment were implemented with $N_{\text{MC}} = 2000$, $N_{\text{bi}} = 1500$.

The performance unmixing algorithms in terms of abundance estimation is evaluated by

¹we extracted these endmembers from the spectral libraries of the ENVI software [18]

computing the root normalised mean square error (RNMSE) defined by

$$\text{RNMSE} = \sqrt{\frac{1}{N_{\text{row}}N_{\text{col}}R} \sum_{i,j} \|\mathbf{a}_{i,j} - \widehat{\mathbf{a}}_{i,j}\|^2} \quad (27)$$

where $\mathbf{a}_{i,j}$ and $\widehat{\mathbf{a}}_{i,j}$ are the true and estimated abundance vectors for the pixel (i, j) of the image.

For this scenario, the proposed G-RCA algorithm is compared with the classical NCLS algorithm [1] assuming the LMM (without sum-to-one constraint (STO)), comparisons to nonlinear SU methods will be addressed in scenario 2 described below. The results obtained with G-RCA, G-RCA+ and NCLS are 1.04×10^{-2} , 1.04×10^{-2} and 0.97×10^{-2} respectively. We observe that the three methods performed similarly, showing that using G-RCA+ to analyse linearly mixed pixels does not degrade significantly the estimation performance.

By analysing the distribution of the estimated nonlinearity levels $\widehat{\mathbf{s}}_{i,j}^2$ (computed by approximating the expectation $\text{E}[\mathbf{s}_{i,j}^2 | \mathbf{Y}, \hat{\alpha}_3]$) we confirm that G-RCA/G-RCA+ correctly identifies linearly mixed pixels. Indeed, the mean and variance of the estimated nonlinearity levels (computed by polling the 10000 pixels) are 1.4×10^{-4} and 1.9×10^{-7} for G-RCA and 2.0×10^{-5} and 4.2×10^{-9} for G-RCA+, confirming that the amplitude of the nonlinear coefficients are significantly smaller than that of the abundances. It is also worth mentioning that unlike NCLS, G-RCA/G-RCA+ is able to handle unknown coloured noise (i.e., frequency-dependent noise levels).

B. Second scenario: Nonlinear mixtures

Data Set:

The objective here is to evaluate the performance of the proposed model when applied to images containing different kinds of linear and nonlinear mixtures. We consider a synthetic image of 100×100 pixels generated with the same $R = 3$ endmembers of the previous experiment, but using 6 different mixing models. More precisely, we have used a Potts-Markov random field (with parameter $\beta = 1.6$) to generate a spatially coherent partition of the image where each partition is assigned to one of the 6 mixing models, which was then used to generate the observations for that partition of the image, (the map with the mixing model assigned to each pixel is depicted in Fig. 3 (a)). The class \mathcal{C}_1 (resp. \mathcal{C}_2) is associated the LMM without (resp. with) abundance STO (LMM-WSTO and LMM-STO, respectively). The pixels of class \mathcal{C}_3 have been generated according to the generalized bilinear mixing

model (GBM) [6]

$$\mathbf{y}_{i,j} = \sum_{r=1}^R a_{r,i,j} \mathbf{m}_r + \sum_{k=1}^{R-1} \sum_{k'=k+1}^R \gamma_{i,j}^{(k,k')} a_{k,i,j} a_{k',i,j} \mathbf{m}_k \odot \mathbf{m}_{k'} + \mathbf{e}_{i,j} \quad (28)$$

with $\gamma_{i,j}^{(k,k')} = 1$, which corresponds to the model investigated in [13] (Fan's model). The class \mathcal{C}_4 is composed of pixels generated according to the PPNMM [8] as follows

$$\mathbf{y}_{i,j} = \mathbf{M} \mathbf{a}_{i,j} + b (\mathbf{M} \mathbf{a}_{i,j}) \odot (\mathbf{M} \mathbf{a}_{i,j}) + \mathbf{e}_{i,j}. \quad (29)$$

with $b = 0.2$. The pixels of the class \mathcal{C}_5 have been generated using the bilinear model investigated in [5], referred to as Nascimento's model (NM) and defined as

$$\mathbf{y}_{i,j} = \sum_{r=1}^R a_{r,i,j} \mathbf{m}_r + \sum_{k=1}^{R-1} \sum_{k'=k+1}^R \gamma_{i,j}^{(k,k')} \mathbf{m}_k \odot \mathbf{m}_{k'} + \mathbf{e}_{i,j} \quad (30)$$

where the mixture coefficients (associated with the linear and nonlinear terms) of each pixel sum to one. Finally, the class \mathcal{C}_6 has been generated according to (1) with zero-mean Gaussian nonlinearity coefficients with variance $s_{i,j}^2 = 0.1$. Note that \mathcal{C}_6 is the only class allowing for negative nonlinearities. For the classes \mathcal{C}_2 , \mathcal{C}_3 and \mathcal{C}_4 (whose underlying models rely on the abundance STO assumption), the abundance vectors have been randomly generated according to a uniform distribution over the admissible set defined by the positivity and sum-to-one constraints. The mixing coefficients in (30) (for the pixels of \mathcal{C}_5) have been uniformly generated in the simplex defined by the positivity and STO constraints. The abundances of the pixels in \mathcal{C}_1 and \mathcal{C}_6 have been generated according to (4) with $\beta_r = 0.3, \forall r$. All pixels have been corrupted by additive i.i.d Gaussian noise of variance $\sigma^2 = 3 \times 10^{-4}$, corresponding to an average signal-to-noise ratio SNR 29dB. The noise is assumed to be i.i.d. for a fair comparison with SU algorithms assuming i.i.d. Gaussian noise. Fig. 3 (b) shows the log-energy of the nonlinear contribution for each pixel of the image, i.e., $\log(\phi_{i,j})$.

Unmixing:

Different estimation procedures have been considered for the four different mixing models:

- The NCLS algorithm [1] which is known to have good performance for linear mixtures when the abundance STO assumption can be relaxed.
- The FCLS algorithm [1] which is known to have good performance for linear mixtures and relying on the abundance STO.
- The GBM-based optimization approach [6] which is adapted for bilinear nonlinearities. The optimization algorithm is stopped when the norm of the difference between consecutive parameter estimates is smaller than 10^{-6} .

		C_1	C_2	C_3	C_4	C_5	C_6
		(LMM-WSTO)	(LMM-STO)	(GBM)	(PPNM)	(NM)	(RCA)
SU Algo.	NLCS	0.98	0.96	5.11	5.10	10.38	26.35
	FLCS	81.45	0.59	11.57	9.90	32.51	30.40
	GBM	80.68	0.60	4.64	5.01	32.54	29.25
	PPNM	70.33	1.11	1.85	0.97	28.13	23.08
	NM	81.06	0.98	11.53	9.77	2.73	29.43
	RCA	1.12	1.09	2.69	2.62	3.63	6.85
	G-RCA	1.34	1.29	2.69	2.65	3.56	6.96
	G-RCA+	1.21	1.14	2.11	2.86	2.88	19.63

TABLE I. SCENARIO 2: ABUNDANCE RNMSES ($\times 10^{-2}$).

		C_1	C_2	C_3	C_4	C_5	C_6
		(LMM-WSTO)	(LMM-STO)	(GBM)	(PPNM)	(NM)	(RCA)
SU Algo.	NLCS	1.72	1.72	1.81	1.78	2.07	4.43
	FLCS	55.12	1.72	2.61	2.49	7.65	11.69
	GBM	54.54	1.72	1.92	2.01	7.65	11.28
	PPNM	9.47	1.72	1.73	1.72	3.26	4.00
	NM	55.09	1.73	2.62	2.62	1.71	9.97
	RCA	1.72	1.71	1.70	1.71	1.70	1.70
	G-RCA	1.72	1.71	1.70	1.71	1.70	1.70
	G-RCA+	1.72	1.72	1.72	1.72	1.72	3.60

TABLE II. SCENARIO 2: RECONSTRUCTION ERRORS ($\times 10^{-2}$).

- The gradient-based approach of [8] which is based on a PPNMM and has shown nice properties for various polynomial nonlinearities.
- The FCLS algorithm used with an extended endmember matrix (containing the bilinear products of the endmembers) for unmixing based on the NM. This algorithm is denoted by NM is the remainder of the paper.
- The RCA algorithm proposed in [10] with $K = 6$ classes, $N_{MC} = 3000$, $N_{bi} = 200$ and $\beta = 1.6$ (β is the granularity parameter of the Potts model used in [10] for nonlinearity-based segmentation).
- The proposed G-RCA/G-RCA+ with $N_{MC} = 2000$, $N_{bi} = 1500$.

The abundance estimation performance of 6 unmixing strategies is evaluated using the RN-MSE obtained for each class of pixels and defined by

$$\text{RNMSE}_k = \sqrt{\frac{1}{N_k R} \sum_{(i,j) \in I_k} \|\mathbf{a}_{i,j} - \hat{\mathbf{a}}_{i,j}\|^2} \quad (31)$$

where I_k is the set of indices of the pixels in the class \mathcal{C}_k and N_k is the number of pixels in \mathcal{C}_k . The results obtained by the 6 algorithms and are presented in Table I which shows that the RCA model (1) leads to robust abundance estimation algorithms since RCA, G-RCA and G-RCA+ provide satisfactory results for the 6 different mixtures. Moreover, RCA, G-RCA provide similar results which confirms that the generalization of RCA (fixed number of classes) to G-RCA does not significantly degrade the abundance estimation performance, while allowing more general spatial variations of the nonlinearities. These results also show that G-RCA+ generally provides better abundance estimates than G-RCA when the nonlinearities are non-negative. The nonlinearity level map estimated by G-RCA and G-RCA+, built from the estimates of $\{\|\phi_{i,j}\|^2\}$ and depicted in Fig. 3, (c) and (d) respectively, show that the proposed algorithms are able to correctly identify the regions where nonlinear effects occur and that G-RCA+ generally provides better estimated nonlinearity energies for positive nonlinearities due to the additional positivity constraints.

The image reconstruction performance of the SU algorithms is evaluated using average reconstruction error (RE) for each class of pixels and defined by

$$\text{RE}_k = \sqrt{\frac{1}{N_k L} \sum_{(i,j) \in I_k} \|\mathbf{y}_{i,j} - \hat{\mathbf{y}}_{i,j}\|^2} \quad (32)$$

where $\hat{\mathbf{y}}_{i,j}$ is the (i, j) th reconstructed pixel. The reconstruction errors in Table II show that that RCA and G-RCA are flexible enough to handle the 6 different models associated with the 6 classes considered. More precisely, the reconstruction errors provided by RCA and G-RCA correspond to the standard deviation of the additive Gaussian noise ($\sigma^2 = 3 \times 10^{-4}$). G-RCA+ also provides accurate reconstructions errors, expect for class \mathcal{C}_6 , because G-RCA+ is not able to capture negative nonlinearities.

Bayesian detection of nonlinearity

As explained previously, the proposed MCMC algorithm can be used to detect image pixels with significant nonlinear mixing (this is formulated as a Bayesian hypothesis test involving the posterior probability (14)). In order to illustrate this, Fig. 5 compares the true nonlinearity presence map (depicted in Fig. 5 (a)) with the probabilities (18) estimated with G-RCA+ and $\eta = 2$ (Fig. 5 (b)) and the corresponding detection map (Fig. 5 (c)) for the synthetic image

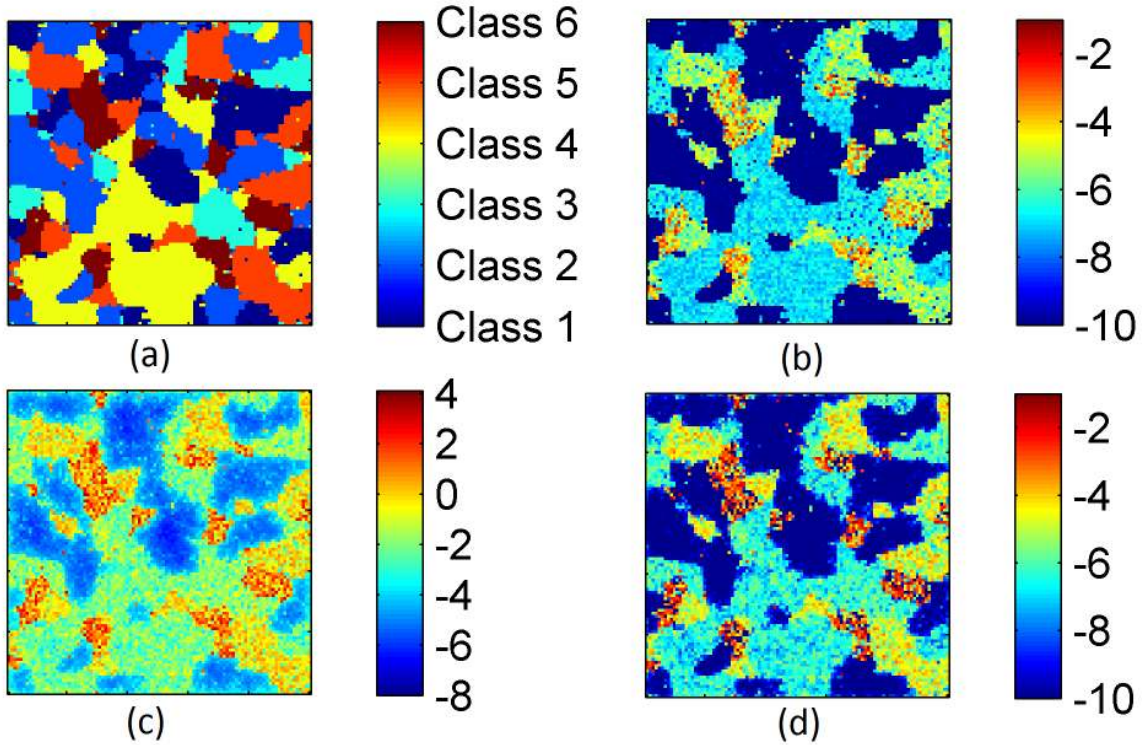


Fig. 3. Nonlinear unmixing: (a) Mixing model (class) allocation, (b) true log-energy of the nonlinear effects, (c)-(d) nonlinear log-energy estimated with G-RCA and with G-RCA+.

considered in Scenario 2. Recall that the detection map is computed by thresholding the probability map (we used $a_0 = a_1$ leading to a threshold value of 0.5). It is worth noting that both η in (14) and the loss function coefficients a_0, a_1 are application specific and can be adjusted to reflect prior knowledge about the confidence in the model for a specific scene, the probability of nonlinear effects, and the relative cost of false positive (false alarm) and false negative detections. Moreover, Table III shows the the empirical probability of false alarm P_{FA} and probability of detection P_D computed with G-RCA+ for this experiment and using different values of η . We observe the good performance of G-RCA+, which for $\eta = 1$ is able to detect over 85% of nonlinearly mixed pixels with a probability of false alarm of 0.5%. Finally, it is of note that unlike the original RCA algorithm [10], the Bayesian model proposed in this paper does not allocate prior probability to the specific case of linearly mixed pixels (i.e., the case $\phi_{i,j} = 0$ has prior density but not prior mass). As a result, it is not possible to perform Bayesian point hypothesis tests (i.e., $\phi_{i,j} = 0$ vs $\phi_{i,j} \neq 0$) that are possible with RCA. The development of a new Bayesian model and Bayesian tests that

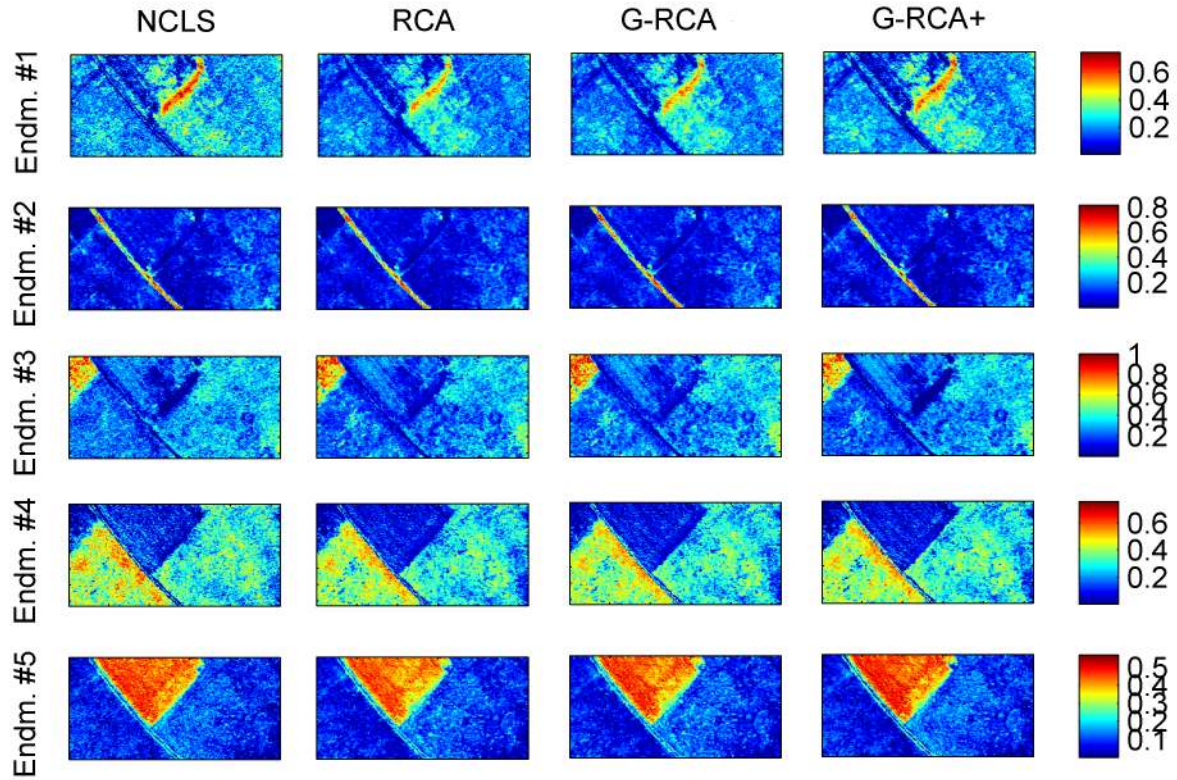


Fig. 4. Abundance maps estimated with NCLS, RCA, G-RCA and G-RCA+ (from left to right) for the Villelongue real image.

combine the strengths of both approaches is currently under investigation.

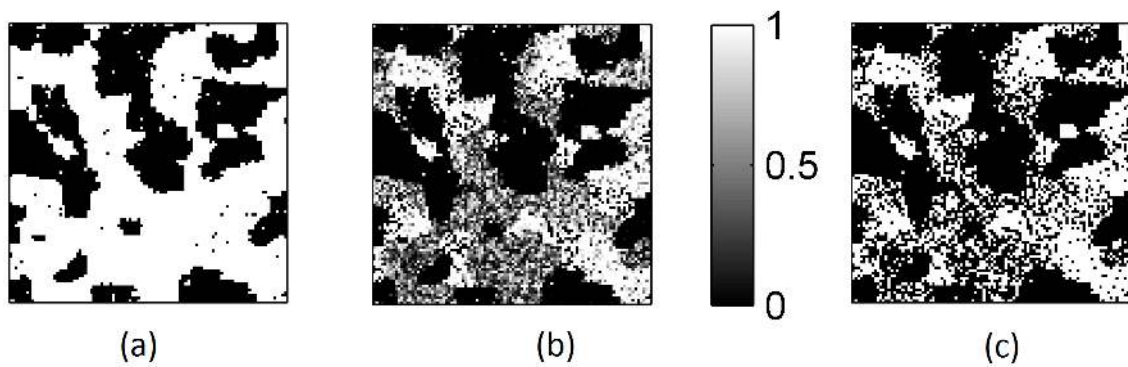


Fig. 5. Nonlinear mixing detection in the synthetic image of Scenario 2: (a) Nonlinearity presence/absence (ground truth), (b) Posterior probability of significant nonlinearities $P_{i,j}$ estimated with G-RCA+ using (14), (c) Bayesian hypothesis test for nonlinearity detection ($P_{i,j} > 1/2$).

	$\eta = 1$	$\eta = 1.5$	$\eta = 2$	$\eta = 2.5$	$\eta = 3$
$P_{FA}(\times 10^{-2})$	0.53	0.15	0.30	0.02	0
$P_D(\times 10^{-2})$	85.83	78.93	72.33	66.15	60.95

TABLE III. SCENARIO 2: DETECTION PERFORMANCE.

VI. SIMULATIONS: REAL HYPERSPECTRAL IMAGE

This section presents an application of the proposed G-RCA method to a real hyperspectral image. The hyperspectral image considered in this experiment was acquired in 2010 by the Hypspx hyperspectral scanner over Villelongue, France ($00^{\circ}03'W$ and $42^{\circ}57'N$). This scene was observed at $L = 160$ spectral bands ranging from the visible to near infra-red with a spatial resolution of 0.5m. This dataset has already been studied in [9], [10], [19], [20] and is mainly composed of forested and urban areas (see [19] for more details about the data acquisition and pre-processing steps). We have applied our method to the region of interest of size 180×250 pixels that is depicted in Fig. 6 (a). This region is composed mainly of a path and different vegetation species and has $R = 5$ endmembers, whose spectral signatures have been extracted from the data using VCA [21].

Figs. 6 (c) and (d) show the nonlinearity levels estimated with the proposed G-RCA/G-RCA+ method. For comparison, the results obtained with RCA [10] are presented in Fig. 6 (d) (recall that to simplify the estimation problem, RCA artificially constrains nonlinearities to take a finite number of values (5 here)). Since RCA does not directly estimate $\{\|\phi_{i,j}\|^2\}$ but $\{\|s_{i,j}\|^2\}$, Figs. 6 (c) and (d) depicts the minimum mean square error estimator of the pixel-wise nonlinearity level

$$\hat{\mathbf{S}}_{MMSE} = \mathbf{E}[\mathbf{S}|\mathbf{Y}, \hat{\alpha}_3], \quad (33)$$

where the expectation is now taken with respect to the marginal posterior density $f(\mathbf{S}|\mathbf{Y}, \alpha_3)$. In a similar fashion to the abundance estimators, these estimators are approximated using Monte Carlo using

$$\hat{\mathbf{S}}_{MMSEj} = \frac{1}{N_{MC} - N_{bi}} \sum_{t=N_{bi}+1}^{N_{MC}} \mathbf{S}^{(t)}. \quad (34)$$

We observe that the results obtained with both methods are in good visual agreement and highlight spatial structures that can be easily identified in the colour image (e.g., path) where one would expect nonlinear mixing to occur. More importantly, by not constraining the number of nonlinearity levels, G-RCA and G-RCA+ to produce spatially smooth estimates

that are realistic (and that do not require specification of the number of nonlinearity levels a priori). It is important to note that the results obtained with G-RCA+ indicate that the nonlinear effects in the image are sparser and weaker than previously suggested by RCA (and G-RCA). Due to the high correlation between the nonlinear terms (cross-products of the endmembers) as well as their energy, the estimation of the nonlinear coefficients is difficult, particularly for RCA and G-RCA that do not take into account the positivity of Γ . Indeed, in the model used in RCA and G-RCA Γ can take large positive and negative values which average out, leading to large estimated nonlinearity levels. By constraining the nonlinear coefficients to be non-negative, G-RCA+ yields smaller and sparser nonlinearity levels that are arguably closer to the ground truth. Finally, Figs. 6 (e)-(f) show the estimated posterior probability of nonlinear mixing computed using (14) (with $\eta = 2$) and the nonlinear mixing detection results (computed by thresholding the probabilities w.r.t. 0.5). Again, nonlinearly mixed pixels are clearly identified near the path and at the boundary between two fields where we expect nonlinear mixing to occur.

Moreover, Fig. 4 shows that the abundances estimates obtained with RCA, G-RCA, G-RCA+ and with the NCLS algorithm. Note that there is no abundance ground truth for this image making it difficult to quantify abundance estimation precision directly. However, this figure shows that algorithm based on the RCA model provide abundance maps generally in agreement with those obtained with NCLS, although the results can vary locally (e.g, abundances of the first endmember between the two fields). We implemented G-RCA(+) using $N_{MC} = 2000$ and $N_{bi} = 1500$ (computing these results using MATLAB required 7 hours on a 3GHz Intel Xeon quad-core workstation). We observe that G-RCA and G-RCA+ perform similarly to the RCA algorithm, while not requiring fixing a number of classes. Finally, Table 1 reports the reconstruction errors of each algorithm ($RE = \sqrt{(\sum_{i,j} \|\hat{y}_{i,j} - y_{i,j}\|^2) / (N_{row} N_{col} L)}$). For completeness we also include the reconstruction errors of the linear SU algorithm NCLS[1] and the nonlinear SU algorithms GBM [22] and PPNMM [8]. We observe that G-RCA performs similarly in terms of RE to other state of the art algorithms.

G-RCA	G-RCA+	RCS	K-HYPE	NCLS	GBM	PPNMM
0.22	0.22	0.22	0.22	0.22	0.22	0.22

TABLE IV. RECONSTRUCTION ERRORS ($\times 10^{-2}$).

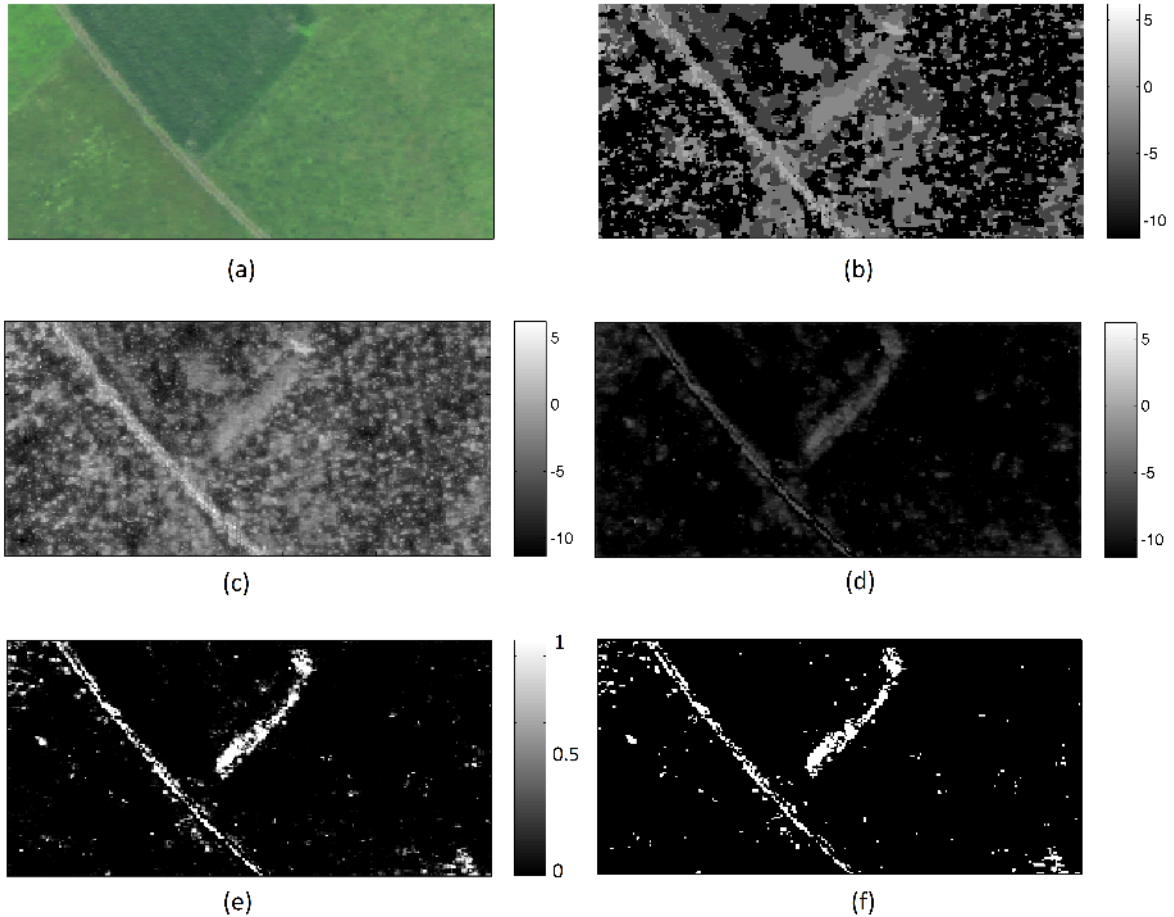


Fig. 6. Nonlinearity level estimation: (a) True colour image of the scene of interest. Levels of nonlinearity estimated with RCA (using $K = 5$ levels) (b), with G-RCA (c) and with G-RCA+ (d). (e) G-RCA+ estimation of posterior probability of significant nonlinear mixing (14) ($\eta = 2$), and (f) nonlinear mixing detection map.

VII. CONCLUSION

This paper has presented a new hierarchical Bayesian algorithm for spectral unmixing of hyperspectral images which incorporates the spatial dependencies inherent in an image associated with the nonlinear mixture effects. The nonlinear mixtures were decomposed into a linear combination of the endmembers and an additive term which represents the nonlinear effects. This term was further decomposed as a combination of the endmembers cross-products. A Gamma Markov random field was introduced to promote smooth nonlinearity variations in the image. In contrast with previously reported work where nonlinear unmixing relied on a nonlinearity level-based image segmentation, the proposed model allows the level of nonlinearity to differ in each pixel while allowing the identification of regions where

nonlinear effects occur. In this paper, a zero-mean Gaussian prior, restricted to the positive orthant was assigned to the nonlinear coefficients of each pixel. This choice was motivated by the fact that several existing models include positivity constraints for the nonlinear terms, e.g. [4]–[6], include such constraints within the SU procedure, and this was previously not possible using the RCA model in [10] due to the marginalisation of these parameters. The results presented in this paper have shown that it can significantly improve the unmixing performance. In this paper, the endmembers were assumed to be perfectly known but often need to be extracted from the data. Future work will include the generalization of the G-RCA+ model to account for endmember estimation errors and more general sources of nonlinearity (such as endmember intrinsic variability).

REFERENCES

- [1] D. C. Heinz and C.-I. Chang, “Fully constrained least-squares linear spectral mixture analysis method for material quantification in hyperspectral imagery,” *IEEE Trans. Geosci. and Remote Sensing*, vol. 29, no. 3, pp. 529–545, March 2001.
- [2] J. M. Bioucas-Dias, A. Plaza, N. Dobigeon, M. Parente, Q. Du, P. Gader, and J. Chanussot, “Hyperspectral unmixing overview: Geometrical, statistical, and sparse regression-based approaches,” *IEEE J. Sel. Topics Appl. Earth Observations Remote Sensing*, vol. 5, no. 2, pp. 354–379, April 2012.
- [3] B. W. Hapke, “Bidirectional reflectance spectroscopy. I. Theory,” *J. Geophys. Res.*, vol. 86, pp. 3039–3054, 1981.
- [4] B. Somers, K. Cools, S. Delalieux, J. Stuckens, D. Van der Zande, W. W. Verstraeten, and P. Coppin, “Nonlinear hyperspectral mixture analysis for tree cover estimates in orchards,” *Remote Sensing of Environment*, vol. 113, no. 6, pp. 1183–1193, 2009.
- [5] J. M. P. Nascimento and J. M. Bioucas-Dias, “Nonlinear mixture model for hyperspectral unmixing,” in *Proc. SPIE Image and Signal Processing for Remote Sensing XV*, L. Bruzzone, C. Notarnicola, and F. Posa, Eds. 2009, vol. 7477, p. 74770I, SPIE.
- [6] A. Halimi, Y. Altmann, N. Dobigeon, and J.-Y. Tourneret, “Nonlinear unmixing of hyperspectral images using a generalized bilinear model,” *IEEE Trans. Geosci. and Remote Sensing*, vol. 49, no. 11, pp. 4153–4162, Nov. 2011.
- [7] J. Chen, C. Richard, and P. Honeine, “Nonlinear unmixing of hyperspectral data based on a linear-mixture/nonlinear-fluctuation model,” *IEEE Trans. Signal Process.*, vol. 61, no. 2, pp. 480–492, 2013.
- [8] Y. Altmann, A. Halimi, N. Dobigeon, and J.-Y. Tourneret, “Supervised nonlinear spectral unmixing using a postnonlinear mixing model for hyperspectral imagery,” *IEEE Trans. Image Processing*, vol. 21, no. 6, pp. 3017–3025, June 2012.
- [9] Y. Altmann, N. Dobigeon, and J.-Y. Tourneret, “Unsupervised post-nonlinear unmixing of hyperspectral images using a Hamiltonian Monte Carlo algorithm,” *IEEE Trans. Image Processing*, vol. 23, no. 6, pp. 2663–2675, June 2014.
- [10] Y. Altmann, N. Dobigeon, S. McLaughlin, and J.-Y. Tourneret, “Residual component analysis of hyperspectral images - application to joint nonlinear unmixing and nonlinearity detection,” *IEEE Trans. Image Processing*, vol. 23, no. 5, pp. 2148–2158, May 2014.
- [11] A. Kalaitzis and N. D. Lawrence, “Residual components analysis,” in *Proc. Int. Conf. Mach. Learning (ICML)*, 2012.

- [12] O. Dikmen and AT. Cemgil, “Gamma markov random fields for audio source modeling,” *IEEE Trans. Audio, Speech, Language Processing*, vol. 18, no. 3, pp. 589–601, March 2010.
- [13] W. Fan, B. Hu, J. Miller, and M. Li, “Comparative study between a new nonlinear model and common linear model for analysing laboratory simulated-forest hyperspectral data,” *Remote Sensing of Environment*, vol. 30, no. 11, pp. 2951–2962, June 2009.
- [14] Marcelo Pereyra, Nick Whiteley, Christophe Andrieu, and Jean-Yves Tournet, “Maximum marginal likelihood estimation of the granularity coefficient of a Potts-Markov random field within an mcmc algorithm,” in *Proc. IEEE-SP Workshop Stat. and Signal Processing*, Gold Coast, Australia, July 2014.
- [15] M. Pereyra, N. Dobigeon, H. Batatia, and J.-Y. Tournet, “Estimating the granularity coefficient of a Potts-Markov random field within an MCMC algorithm,” *IEEE Trans. Image Processing*, vol. 22, no. 6, pp. 2385–2397, June 2013.
- [16] C. P. Robert and G. Casella, *Monte Carlo Statistical Methods*, Springer-Verlag, New York, second edition, 2004.
- [17] A. Pakman and L. Paninski, “Exact Hamiltonian Monte Carlo for Truncated Multivariate Gaussians,” *ArXiv e-prints*, Aug. 2012.
- [18] RSI (Research Systems Inc.), *ENVI User’s guide Version 4.0*, Boulder, CO 80301 USA, Sept. 2003.
- [19] D. Sheeren, M. Fauvel, S. Ladet, A. Jacquin, G. Berton, and A. Gibon, “Mapping ash tree colonization in an agricultural mountain landscape: Investigating the potential of hyperspectral imagery,” in *Proc. IEEE Int. Conf. Geosci. and Remote Sensing (IGARSS)*, July 2011, pp. 3672–3675.
- [20] Y. Altmann, N. Dobigeon, S. McLaughlin, and J. Tournet, “Nonlinear spectral unmixing of hyperspectral images using Gaussian processes,” *IEEE Trans. Signal Process.*, vol. 61, no. 10, pp. 2442–2453, May 2013.
- [21] José M.P. Nascimento and José M. Bioucas-Dias, “Vertex component analysis: A fast algorithm to unmix hyperspectral data,” *IEEE Trans. Geosci. and Remote Sensing*, vol. 43, no. 4, pp. 898–910, April 2005.
- [22] A. Halimi, Y. Altmann, N. Dobigeon, and J.-Y. Tournet, “Unmixing hyperspectral images using a generalized bilinear model,” in *Proc. IEEE Int. Conf. Geosci. and Remote Sensing (IGARSS)*, July 2011, pp. 1886 –1889.